Bulletin of Electrical Engineering and Informatics
Vol. 10, No. 4, August 2021, pp. 1914~1922
ISSN: 2302-9285, DOI: 10.11591/eei.v10i4.3085

Applying SiO_2 nano-particles for improving optical properties of WLED conformal and in-cup structures

Phan Xuan Le, Pham Quang Minh
Faculty of Engineering, Van Lang University, Viet Nam

Article Info

Article history:

Received Dec 24, 2020
Revised Apr 18, 2021
Accepted Jun 14, 2021

Keywords:

Color uniformity
Luminous flux
Mie-scattering theory
SiO_2

ABSTRACT

This article is the analysis of SiO_2 nano-particles' influences on the luminous efficiency and the color temperature uniformity of a remote phosphor structure in a WLED. The purpose of integrating SiO_2 into the silicone layer in the remote phosphor structure is to significantly promote the scattering occurrences. Particularly, with an appropriate proportion of SiO_2, there could be more blue lights generated at large angles, leading to reducing the angular-dependent color temperature deviation. The luminous flux also can get benefits from SiO_2 addition owing to a proper air-phosphor layer refractive index ratio provided by this SiO_2/silicone compound. The attained experimental results were compared with optical values of a non-SiO_2 remote phosphor configuration and showed a notable enhancement. The color deviation was reduced by approximately 600 K in the angles from -70^0 to 70^0. Additionally, the lumen efficiency was improved by 2.25% at 120 mA driving current. Hence, SiO_2 can be used to boost both color uniformity and luminous efficacy for remote-phosphor WLED.

Corresponding Author:

Phan Xuan Le
Faculty of Engineering
Van Lang University
No. 45 Nguyen Khac Nhu Street, Ho Chi Minh City, Vietnam
Email: le.px@vlu.edu.vn

1. INTRODUCTION

As the environmental issue has been a global concern, utilizing a lighting source that is eco-friendly but still excellent in lighting efficiency is in high demand. To serve this purpose, lighting emitting diodes (LEDs) has been applied to various illuminating devices as a replacement for incandescent bulbs and fluorescent lamps which are inferior in optical performance and contain mercury [1]-[4]. To generate white light, LED package is usually fabricated using phosphors to down-convert blue lights emitted from a LED chip. One of the first and most common LED package in use is the YAG:Ce-based InGaN LED in which YAG:Ce is the $Y_3Al_5O_{12}$:Ce yellow phosphor applied for blue-light down conversion. This LED results in a cold and low color-rendering-index white light as well as emits high correlated color temperature (CCT). Thus, figuring out a way to improve the color rendering index (CRI) and lower the CCT for YAG:Ce-based white LEDs (WLEDs) has drawn extensive attention from researchers. It is reported that the mixture of red and yellow phosphors could promote the color adequacy but sharply degrade the luminescence efficiency [5]-[8]. Accordingly, to achieve better color quality, the reduction in lumen output of white LED is unavoidable, yet researchers had been working on how to minimize this luminous loss while heightening the color quality simultaneously. The application of semiconductor nanocrystals or quantum dots (QDs) has been introduced to modify the emission spectra for achieving a reduction in luminescence loss of traditional WLEDs [9]-[13]. The advantage of using QDs is the tunable emission wavelength which is managed by their

narrow emission spectra [14], [15], helping the high-power WLED achieve high color rendering index (CRI). However, to fully take advantage of QDs, it must be mixed uniformly with the silicone polymer in the fabricating procedure. In addition to that, the long chain and hydrophobic surface ligands on QDs could disturb the forming process of polymer chains, degrade the stability of mechanical properties of the package, and result in poor compatibility with silicone polymers having a very polar chain [16]. In an attempt to resolve this problem along with supporting the CRI development of WLEDs, Ziegler and his team introduced an encapsulation of QDs blended with silica-based nanocomposites [17]-[19]. Silica-based composite is one of nanocrystal based inorganic nanocomposites that researchers have been greatly interested in because their physical and chemical features could be appropriate for being applied in many applications, including WLED devices [20]-[22]. Various investigations have been carried out to uniformly mixing the silica with QDs. A traditional approach for the incorporation of QDs in silica is to employ Stöber method to grow the silica shell on semiconductor nanocrystals, after its ligand surface is exchanged for the hydrophilic surface [23]. Nevertheless, there is the limitation of the blended nanocrystals number in each nanocomposite particle [24], so it is essential to add high-concentration SiO_2 multiple nanocrystals to synthesize phosphor material with high luminescence [25]. Thus, another popular method called reverse microemulsion method was utilized for synthesizing SiO_2 nanocomposite particle [26], and was able to result in a smooth silica surface and a uniform distribution of SiO_2 and silica materials. This result is attributed to the reduction in reverse micelle formation and hydrolysis/condensation of the silica precursors by adding surfactants. Capturing this idea, we added SiO_2 nanoparticles to the silicone composite of the remote phosphor structure of WLED and examined its influences on the optical performances of WLEDs. The organization of the study is as follows. In the next section, section 2, the simulation of a SiO_2/silicone packaging WLED is demonstrated, and then the scattering analysis is carried out via a mathematic system that is built based on Mie-scattering theory. Section 3 is about the attained results and discussion. Section 4 is the conclusion that summarized all the findings presented in the whole study.

2. EXPERIMENTAL DETAILS

2.1. MC-WLEDs simulation

The LightTools 9.0 commercial software was applied to carry out the simulation of the WLED using SiO_2-integrated remote phosphor structure which is presented in Figure 1. Figure 1 (a) is the photograph of real LED packages while Figure 1 (b), (c) and (d) are the cross-sectional illustrations of simulated WLED used in this study. The WLED package is comprised of 9 blue LED chips, silicone layer, yellow phosphor $Y_3Al_5O_{12}$ (YAG), and SiO_2 synthesized with silicone composite. Each blue LED chip having 24 mils square, 450 nm peak emission wavelength, and radiant flux of 95 mW at 120 mA driving current. In addition, the yellow-phosphor particle size is set at around 12 μm. The fabrication of the SiO_2/silicone remote phosphor configuration is carried out as the following order. First, the LED chips are bonded onto the plastic lead frame; second, dispense the transparent silicone on the lead frame and cure them at 150°C for an hour. Third, the yellow phosphor particles are mixed with silicone composite to create a slurry of phosphor suspension. Then, spray this slurry on the initial transparent silicone to form the remote phosphor structure. Finally, SiO_2 nanoparticles are integrated into silicone binder and a solvent with alkyl base. After that, the mixture is mixed with or placed above the yellow phosphor composite to complete the desired SiO_2/silicone remote phosphor packaging configuration, as presented in Figure 1 (c) and (d), respectively. It is noted that the concentration of SiO_2 in the silicone composite is about 5% wt.

2.2. Scattering computation

Here, we applied Mie scattering theory and ray tracing method in measurements, so the achieved results can be more precise. Mie theory is a famous tool for scattering computation of WLED optical simulation and has been widely utilized in many commercial optical software, including Lighttools, Tracepro, and ASAP. Usually, optical software considers the scattering of phosphor particles as Mie scattering to perform a simulation of a WLED package, therefore, the revision of Mie scattering computation probably contributes much to improving the performance of the software to give a more accurate simulation of WLED packaging design. The computation of scattering coefficient $\mu_{sca}(\lambda)$, anisotropy factor $g(\lambda)$, and reduced scattering coefficient $\delta_{sca}(\lambda)$ based on Mie theory can be expressed as [25], [26]:

$$\mu_{sca}(\lambda) = \int N(r) C_{sca}(\lambda, r) dr \quad (1)$$

$$g(\lambda) = 2\pi \int_{-1}^{1} \int p(\theta, \lambda, r) f(r) \cos\theta d \cos\theta dr \quad (2)$$

$$\delta_{sca} = \mu_{sca}(1-g) \tag{3}$$

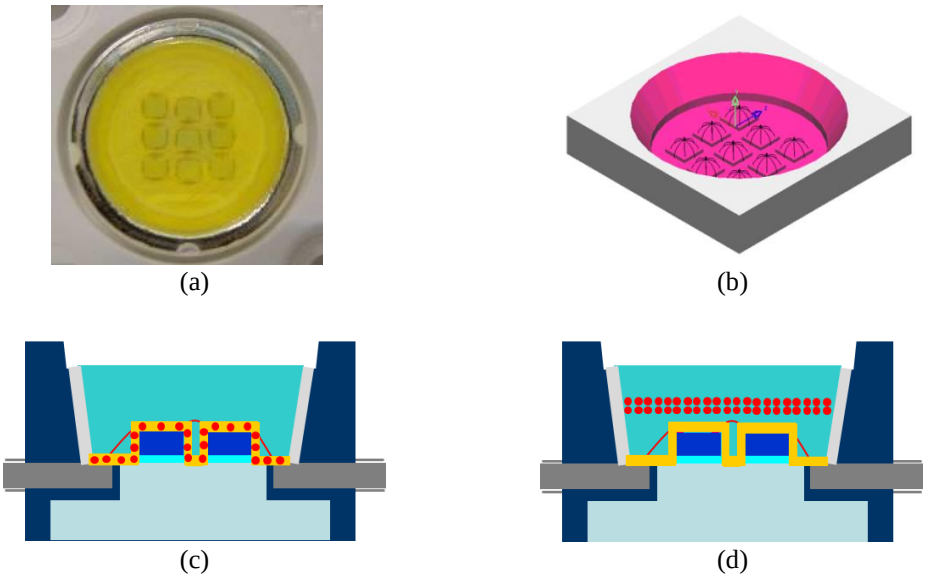

Figure 1. These figures are, (a) photograph of WLEDs sample, (b) the simulated WLEDs model, (c) conformal structure, (d) in-cup structure

In which, $N(r)$ indicates the distribution density of diffusional particles (mm^3), C_{sca} expresses the scattering cross sections (mm^2), $p(\theta,\lambda,r)$ is the phase function, λ is the light wavelength (nm), r is radius of diffusional particles (μm), θ is the scattering angle (°C), and $f(r)$ is the size distribution function of the diffusional particles in the phosphor layer whose calculation can be expressed as follows:

$$f(r) = f_{dif}(r) + f_{phos}(r) \tag{4}$$

$$\begin{aligned} N(r) &= N_{dif}(r) + N_{phos}(r) \\ &= K_N.[f_{dif}(r) + f_{phos}(r)] \end{aligned} \tag{5}$$

As can be seen in (5), $N(r)$ is comprised of $N_{dif}(r)$ and $N_{phos}(r)$, both of which are the diffusional particle density and the phosphor particle density, respectively. $f_{dif}(r)$ and $f_{phos}(r)$ indicate the size distribution function data of the diffusional and phosphor particles, while K_N shows the number of the diffusor unit for one diffusor concentration and can be computed by:

$$c = K_N \int M(r)dr \tag{6}$$

Here, $M(r)$ shows the mass distribution of the diffusive unit, demonstrated as:

$$M(r) = \frac{4}{3}\pi r^3[\rho_{dif} f_{dif}(r) + \rho_{phos} f_{phos}(r)] \tag{7}$$

With $\rho_{diff}(r)$ and $\rho_{phos}(r)$ display the density of diffusor and phosphor crystal.
According to the application of Mie theory, calculating C_{sca} can be carried out as the following expression:

$$C_{sca} = \frac{2\pi}{k^2}\sum_{0}^{\infty}(2n-1)(|a_n|^2 + |b_n|^2) \tag{8}$$

In this C_{sca} calculation, $k=2\pi/\lambda$. Meanwhile, parameters a_n and b_n can be attained with below formulas:

$$a_n(x,m)=\frac{\psi_n^{'}(mx)\psi_n(x)-\mathrm{m}\psi_n(mx)\psi_n^{'}(x)}{\psi_n^{'}(mx)\xi_n(x)-\mathrm{m}\psi_n(mx)\xi_n^{'}(x)} \quad (9)$$

$$b_n(x,m)=\frac{m\psi_n^{'}(mx)\psi_n(x)-\psi_n(mx)\psi_n^{'}(x)}{m\psi_n^{'}(mx)\xi_n(x)-\psi_n(mx)\xi_n^{'}(x)} \quad (10)$$

Here, $x=k.r$, m is the refractive index, while $\psi_n(x)$ and $\xi_n(x)$ are the Riccati-Bessel function.
Accordingly, the relative refractive indices of diffusor and phosphor, indicated by m_{dif} and m_{phos}, respectively, in the silicone are possibly obtained via; $m_{dif}={}^{n_{dif}}/_{n_{sil}}$ and $m_{phos}={}^{n_{phos}}/_{n_{sil}}$. Then the phase function can be expressed as:

$$p(\theta,\lambda,r)=\frac{4\pi\beta(\theta,\lambda,r)}{k^2C_{sca}(\lambda,r)} \quad (11)$$

where $\beta\ (\theta,\lambda,r)$, $S_1(\theta)$ and $S_2(\theta)$ are the angular scattering amplitudes calculated as:

$$\beta(\theta,\lambda,r)=\frac{1}{2}[|S_1(\theta)|^2+|S_2(\theta)|^2] \quad (12)$$

$$S_1=\sum_{n=1}^{\infty}\frac{2n+1}{n(n+1)}\begin{bmatrix}a_n(x,m)\pi_n(\cos\theta)\\+b_n(x,m)\tau_n(\cos\theta)\end{bmatrix} \quad (13)$$

$$S_2=\sum_{n=1}^{\infty}\frac{2n+1}{n(n+1)}\begin{bmatrix}a_n(x,m)\tau_n(\cos\theta)\\+b_n(x,m)\pi_n(\cos\theta)\end{bmatrix} \quad (14)$$

There are various studies on the optical characteristics of WLED with YAG:Ce crystal and the results show that α is diverse in a wide range, which can be attributed to the difference in doped Ce concentrations, methods of growing crystal in the package, and tools used for measurements. In the case of blue lights, the range for α variation is from 3 mm^{-1} to 8 mm^{-1}. Meanwhile, in the case of using YAG:Ce ceramics consisting of small crystal particles, the absorption ability of lights is considerably improved, and α range can be heightened to be more than 15 mm^{-1}. This enhancement in light absorption of YAG:Ce ceramic is the result of various light reflections in the packaging material. In this research, the phosphor crystal is considered to provide high α, so the range of α is from 8 mm^{-1} to 20 mm^{-1} to analyze the scattering coefficients μ_{sca}. Figure 2 presents the calculated result of μ_{sca} based on (1). The scattering coefficient is directly proportional to concentration of the phosphor, which means μ_{sca} increases when increasing the phosphor contents. This indicates that the phosphor concentration significantly affects the color quality of generated white lights.

According to the measurement platform, the emitted blue and converted yellow lights from the LED chip have Lambertian radiation patterns. The lenses used in packaging WLED model is made of BK7 glass from Schott. Inside the two integrating spheres, a diffusional white material with 11.1% absorption and 89.9% scattering properties is sprayed onto the spheres' inner surfaces to collect the transmitted and reflected lights. The ray tracing of the configuration is carried out with Monte Carlo method, while the phosphor material is treated as the Mie scattering material. The Henyey-Greenstein function is utilized to present the approximation of the generated angular scattering because the ray tracing is unable to calculate the direction of light scattering of the phosphor, as shown in Figure 3. The results attained using Mie theory was applied first, and then verified with the ray tracing ones. However, the results from ray tracing demonstrated that differences existed when they were compared with the measurement ones. In ray-tracing results, the transmittance was higher and the blue-light absorption was lower than that in measurement results. These variations can be explained by the lower μ_{abs} and μ_{sca} and the higher $g(\lambda)$, in comparison with the true values. Thus, applying these mentioned approaches in simulations is to accomplish more accurate optical constants by locking one of the three constants while modifying the two others to be near to the measurement results.

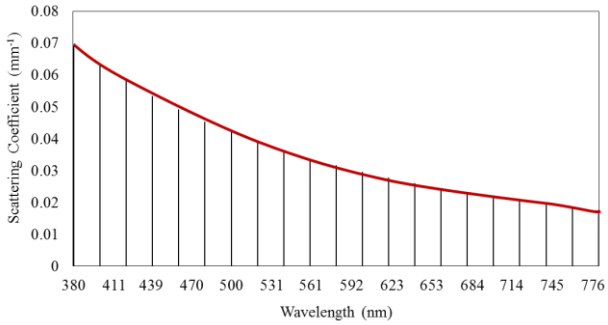

Figure 2. Scattering coefficients of SiO_2 particles

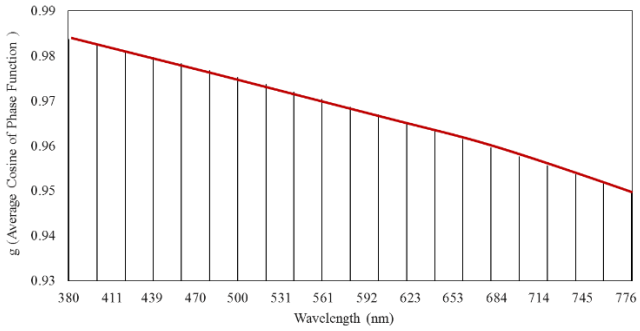

Figure 3. The phase function of SiO_2 particles

3. RESULTS AND DISCUSSION

The definition of angular-dependent CCT uniformity can be demonstrated as CCT_{max}–CCT_{min}. Figure 4 shows the CCT deviation of remote phosphor structures with different weights of SiO_2 particles. As can be seen, when the weight of SiO_2 is 10 mg cm^{-2}, the CCT deviation reaches the lowest values, which means the color uniformity is significantly enhanced. Specifically, the CCT deviation in the SiO_2 remote phosphor package decreases from 1000 K to 420 K, from -70^0 to 70^0 of viewing angles. This 58% improvement of CCT deviation of SiO_2 phosphor package, in comparison with that of conventional phosphor structure, is due to the great scattering ability of SiO_2 that boosts the blue-light extraction at a large angle, allowing the blue and yellow light to be mixed effectively and distributed uniformly. When the weight of SiO_2 passes 10 mg cm^{-2}, the color uniformity would be affected, but is still higher than that of the non-SiO_2 structure. In addition, not only does the chromaticity of white light improve but also the luminous efficiency when the nanoparticle SiO_2 is added to the phosphor configuration.

The luminous flux of SiO_2-doped remote phosphor structure with different weights of SiO_2 is shown in Figure 5. Accordingly, 10 mg cm^{-2} of SiO_2 nanoparticles is optimal for the lumen output of WLED, specifically, the luminous performance increases 2.25%, compared to the result of non-SiO_2 package. The reason is when SiO_2 nanoparticles are integrated into the silicone layer, they can minimize the refractive-index differences at the interface between the air and the phosphor layer. The SiO_2/silicone layer has a refractive index of 1.5, and that parameter of the phosphor layer and the air is 1.8 and 1, respectively. Therefore, a refractive index gradient between the air and phosphor layer can be created using the SiO_2/silicone layer, which leads to higher emitted luminous flux.

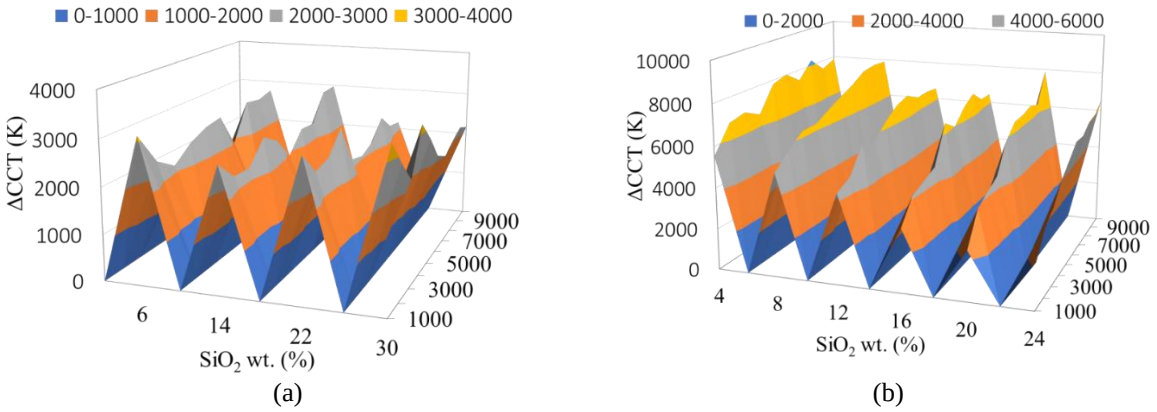

Figure 4. CCT deviations of SiO_2 particles with different diameters, (a) conformal structure, (b) in-cup geometry

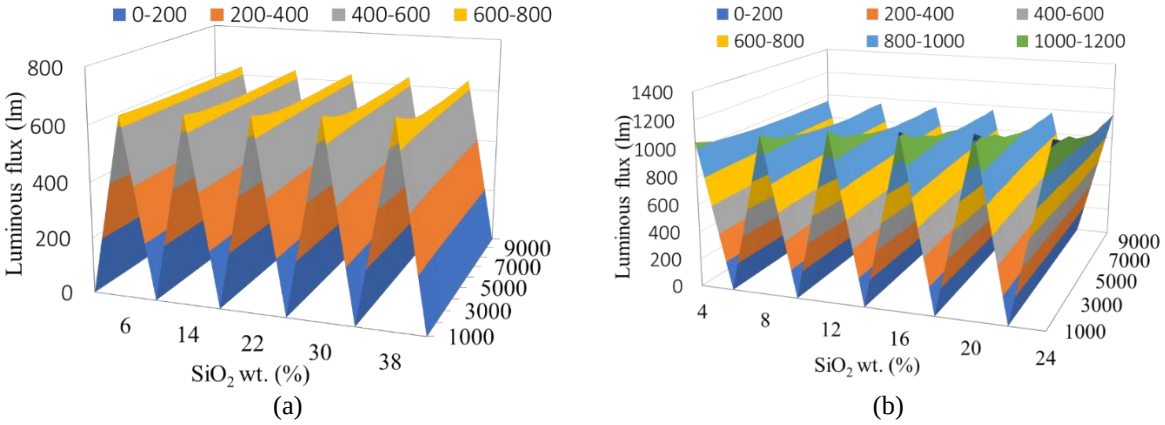

Figure 5. Luminous fluxes of SiO_2 particles with different diameters, (a) conformal structure, (b) in-cup geometry

Next, to understand the effects of SiO_2 on the optical properties of a WLED with phosphor dispensing structure, this study continues demonstrating transmission–absorption and haze experiments. Based on these experiments, the characteristics of SiO_2–phosphor–silicone mixture can be revealed. By comparison with the absorption percentage in the non-SiO_2 dispensing phosphor structure, that in SiO_2-doped dispensing phosphor structure showed a noticiable increase, from about 32% to approximately 42%, at 460 mn wavelength. This indicated that there were more yellow lights converted, leading to promoted luminous efficiency. Besides, after integrating SiO_2 nanoparticle into the silicone layer and placing this composite in the remote phosphor package, different concentrations of SiO_2 probably resulted in the change in obtained optical performance. Additionally, the refractive indices (RI) of silicone, SiO_2, and phosphor are 1.4, 2.23, and 1.8, respectively. Therefore, the calculation of RI of the phosphor layer doping SiO_2 nanoparticle is expressed as:

$$RI=V_1RI_1+V_2RI_2+V_3RI_3 \quad (15)$$

in which, V_1, V_2, and V_3 indicate the concentration of each material in the mixture. The concentrations of SiO_2 mixed in the phosphor/silicon layer are 1% wt. and 3% wt., respectively, so the corresponding RIs of the phosphor layer are 1.428 and 1.445. The influences of the phosphor layer with each RI were investigated via a TFCalc32 simulation. The light extractions in SiO_2-doped phosphor dispensing structure and non-SiO_2 phosphor structure were quite the same as their refractive indices were relatively similar. Therefore, it can be said that the enhancement in luminous output of SiO_2 dispensing configuration depends on SiO_2 scattering ability. Mie-scattering theory was applied to examine the influence of SiO_2 scattering with different concentrations. For this scattering experiment, we presented only SiO_2 nanoparticles, the phosphor is not included, to simplify the model. SiO_2 nanoparticles, having refractive index of 2.23 and a size of 300 nm,

were added into the silicone with 1% wt. and 3% wt. concentrations, respectively. 1% wt. SiO_2 concentration in the silicone composite showed the haze intensity of approximate 100% in the wavelength range below 500 nm, while when the wavelength was above 500 nm, the haze intensity gradually declined, as can be seen in Figure 6. By comparison, we can see that the scattering influences of SiO_2 from the simulated results are compatible with the ones from the experimental outcomes. With higher concentration of SiO_2 added to the silicon, the haze intensity in the wavelength range of 300-700 nm showed a relatively similar trend as the one with lower SiO_2 content. The scattering effects of SiO_2 on the optical performance of WLED are discussed more based on the results of SiO_2 angular-dependent scattering intensity analysis conducted utilizing the full-field finite-difference time-domain (FDTD) simulation. SiO_2 concentration added into the silicone in this study is about 5% wt., and the refractive index of SiO_2/silicone is 1.5. The result of this study demonstrated that 400 nm particle sizes of SiO_2 results in higher scattering intensity in the visible wavelength of incident blue and yellow lights, 450 nm and 560 nm, compared to the results of other sizes. Higher scattering intensity means higher color uniformity, yet it is essential to consider the transmission of blue and yellow lights in the normal light path. After conducted experiments and measurements of SiO_2/silicone layer, it can be realized a constant increase in absorption ability as the concentration of SiO_2 grows. In the case of 300 nm particle size of SiO_2, the absorption can make up from 5% to 15% of light, and this could extent as the SiO_2 diameter becomes larger. Thus, it is impossible to continuously increase the size of SiO_2 particles without any limitation.

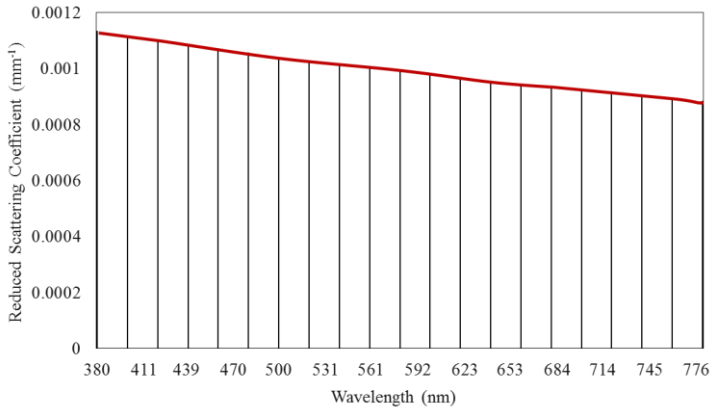

Figure 6. The reduced scattering coefficient of SiO_2 particles at different sizes and wavelength

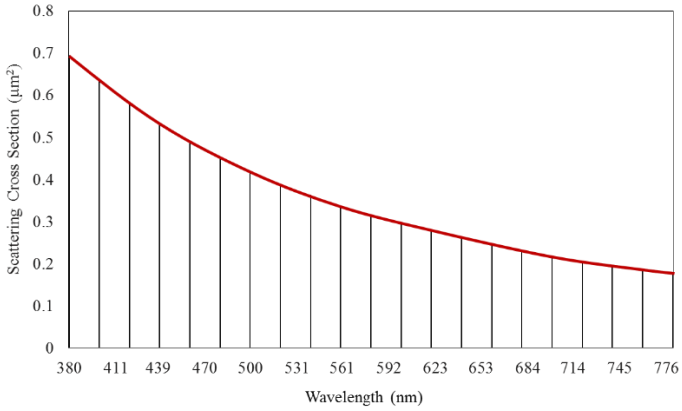

Figure 7. The scattering cross section of SiO_2 particles at different sizes and wavelength

The measurement of angular-dependent relative intensity for blue light and yellow light is carried out to demonstrate the scattering effects of SiO_2 nanoparticles on the emission spectra of the in-cup phosphor structure. The variation of blue light angle in the SiO_2 remote phosphor structure is larger than that in the traditional structure without using SiO_2. This leads to the reduction in blue light transmitting in the normal

direction, which shows that the scattering ability of SiO_2 contributes greatly to minimizing the angular-dependent CCT deviation to enhance the color quality. Meanwhile, the distribution of yellow lights in the non-SiO_2 and SiO_2-doped phosphor structures is nearly identical. The wavelength-dependent haze ratio can explain these results. Given that the weight of SiO_2 is 10 mg cm^{-2}, the haze of yellow lights at the wavelength of 600 nm is 30%, while that of the 450 nm blue light is 35%. It is noted that, the higher the haze ratio, the stronger the scattering of lights, which indicates that the scattering of yellow lights is inferior to the blue-light scattering. This benefits the color distribution and lessens the CCT deviation of the remote phosphor structure doping SiO_2 nanoparticles. According to the haze measurement results illustrated in Figure 5, it is easy to see the diffused component in the wavelength of yellow lights is lower than in the blue-light wavelength, which confirms the idea that the CCT deviation significantly depends on the diversity of blue-light angle in the remote phosphor WLED package. In addition to that, through the measurement of the blue-light weight-dependent relative intensity with various SiO_2 weight at the viewing angle of 70^0, the optimal weight of SiO_2 that can yield the highest blue-light intensity at large angles is recognized at 10 mg cm^{-2}.

4. CONCLUSION

In this research paper, the effects of SiO_2 nanoparticles on the optical performance of remote phosphor structures were analyzed and demonstrated. The Mie-scattering theory and haze measurements were employed to calculate and examine the scattering of SiO_2 particles. From the attained results, the SiO_2 doped structure can enhance the color uniformity by 58%, and luminous efficiency by 2.25% at a driving current of 120 mA, compared to the optical performance of the conventional structure without SiO_2. Moreover, through experimental results, 10 mg cm^{-2} is recognized as the optimal weight of SiO_2 for higher chromatic adequacy and better lumen output of WLED. Hence, SiO_2 can be used to empower the remote phosphor structure to achieve both qualified color uniformity and luminous efficacy for WLED devices.

REFERENCES

[1] N. Bamiedakis, *et al.*, "Ultra-Low Cost High-Density Two-Dimensional Visible-Light Optical Interconnects," *Journal of Lightwave Technology*, vol. 37, pp. 3305-3314, 2019.

[2] L. Xiao, C. Zhang, P. Zhong, G. He, "Spectral optimization of phosphor-coated white LED for road lighting based on the mesopic limited luminous efficacy and IES color fidelity index," *Applied Optics*, vol. 57, no. 4, pp. 931-936, 2018, doi: 10.1364/AO.57.000931.

[3] H. Y. Yu, *et al.*, "Solar spectrum matching with white OLED and monochromatic LEDs," *Applied Optics*, vol. 57, no. 10, pp. 2659-2666, 2018, doi: 10.1364/AO.57.002659.

[4] T. C. Bui, R. Cusani, G. Scarano, M. Biagi, "Metameric MIMO-OOK transmission scheme using multiple RGB LEDs," *Optics Letters*, vol. 26, no. 11, pp. 14038-14050, 2018, doi: 10.1364/OE.26.014038.

[5] X. Huang, *et al.*, "Effect of electron-transfer quenching on the photoluminescence of Pr^{3+} in $MgXO_3$, X = Ge,Si," *Optical Materials Express*, vol. 10, pp. 1163-1168, 2020, doi: 10.1364/OME.389599.

[6] X. Li, D. Kundaliya, Z. J. Tan, M. Anc, N. X. Fang, "Projection lithography patterned high-resolution quantum dots/thiol-ene photo-polymer pixels for color down conversion," *Optics Express*, vol. 27, no. 21, pp. 30864-30874, 2019, doi: 10.1364/OE.27.030864.

[7] T. Shang, Z. P. Sun, Z. Y. Dong, Q. Li, "Network selection method based on MADM and VH-based multi-user access scheme for indoor VLC hybrid networks," *Optics Express*, vol. 26, pp. 30795-30817, 2018, doi: 10.1364/OE.26.030795.

[8] V. Dumont, *et al.*, "Flexure-tuned membrane-at-the-edge optomechanical system," *Optics Express*, vol. 27, no. 18, pp. 25731-25748, 2019, doi: 10.1364/OE.27.025731.

[9] Y. Yuan, *et al.*, "High luminous fluorescence generation using Ce:YAG transparent ceramic excited by blue laser diode," *Optical Materials Express*, vol. 8, no. 9, pp. 2760-2767, 2018, doi: 10.1364/OME.8.002760.

[10] S. R. Chung, C. B. Siao, K. W. Wang, "Full color display fabricated by CdSe bi-color quantum dots-based white light-emitting diodes," *Optical Materials Express*, vol. 8, no. 9, pp. 2677-2686, 2018, doi: 10.1364/OME.8.002677.

[11] Fu-Bang Chen, Kai-Lun Chi, Wei-Yu Yen, Jinn-Kong Sheu, Ming-Lun Lee, and Jin-Wei Shi, "Investigation on Modulation Speed of Photon-Recycling White Light-Emitting Diodes With Vertical-Conduction Structure," *Journal of Lightwave Technology*, vol. 37, no. 4, pp. 1225-1230, 2019.

[12] K. Chung, J. Sui, T. Sarwar, P. C. Ku, "Feasibility study of nanopillar LED array for color-tunable lighting and beyond," *Optics Express*, vol. 27, no. 26, pp. 38229-38235, 2019, doi: 10.1364/OE.382287.

[13] Hisayoshi Daicho, Kiminori Enomoto, Hiroshi Sawa, Satoru Matsuishi, and Hideo Hosono, "Improved color uniformity in white light-emitting diodes using newly developed phosphors," *Optics Express*, vol. 26, no. 19, pp. 24784-24791, 2018, doi: 10.1364/OE.26.024784.

[14] S Rasouli, S Hamzeloui, D Hebri, "Colorful radial Talbot carpet at the transverse plane," *Optics Express*, vol. 27, no. 13, pp. 17435-17448, 2019, doi: 10.1364/OE.27.017435.

[15] X. Liu, *et al.*, "Upconversion luminescence, intrinsic optical bistability, and optical thermometry in Ho^{3+}/Yb^{3+}: $BaMoO_4$ phosphors," *Chinese Optics Letters*, vol. 17, no. 11, pp. 111601-, 2019.

[16] W. Bao, M. Wei, K. Xiao, "Investigating unique hues at different chroma levels with a smaller hue angle step," *Journal of the Optical Society of America A*, vol. 37, no. 4, pp. 671-679, 2020, doi: 10.1364/JOSAA.383002.
[17] W. Zhong, J. Liu, D. Hua, S. Guo, K. Yan, C. Zhang, "White LED light source radar system for multi-wavelength remote sensing measurement of atmospheric aerosols," *Applied Optics*, vol. 58, no. 31, pp. 8542-8548, 2019, doi: 10.1364/AO.58.008542.
[18] H. Lee, S. Kim, J. Heo, W. J. Chung, "Phosphor-in-glass with Nd-doped glass for a white LED with a wide color gamut," *Optics Letters*, vol. 43, no. 4, pp. 627-630, 2018, doi: 10.1364/OL.43.000627.
[19] Y. Fei, J. Zhang, "Luminescence properties of KBaYSi2O7:Ce/Eu-Tb phosphors for multifunctional applications," *Applied Optics*, vol. 58, no.17, pp. 4740-4745, 2019, doi: 10.1364/AO.58.004740.
[20] C. Bai, *et al.*, "Full-color optically-sectioned imaging by wide-field microscopy via deep-learning," *Biomedical Optics Express*, vol. 11, no, 5, pp. 2619-2632, 2020, doi: 10.1364/BOE.389852.
[21] Z. Zhang, W. Yang, "Tunable photoluminescence in $Ba_{1-x}Sr_xSi_3O_4N_2$: Eu^{2+}/ Ce^{3+}, Li^+ solid solution phosphors induced by linear structural evolution," *Optical Materials Express*, vol. 9, no. 4, pp. 1922-1932, 2019, doi: 10.1364/OME.9.001922.
[22] T. Ya. Orudzhev, S. G. Abdullaeva, and R. B. Dzhabbarov, "Increasing the extraction efficiency of a light-emitting diode using a pyramid-like phosphor layer," *Journal of Optical Technology*, vol. 86, no. 10, pp. 671-676, 2019, doi: 10.1364/JOT.86.000671.
[23] Leipeng Li, Yuan Zhou, Feng Qin, Yangdong Zheng, and Zhiguo Zhang, "On the Er^{3+} NIR photoluminescence at 800 nm," *Optics Express*, vol. 28, pp. 3995-4000, 2020, doi: 10.1364/OE.386792.
[24] A. Zhang, *et al.*, "Tunable white light emission of a large area film-forming macromolecular complex with a high color rendering index," *Optical Materials Express*, vol. 8, no. 12, pp. 3635-3652, 2018, doi: 10.1364/OME.8.003635.
[25] X. Hu, *et al.*, "Optimizing selection of the test color sample set for the CIE 2017 color fidelity index," *Optics Express*, vol. 28, no. 6, pp. 8407-8422, 2020, doi: 10.1364/OE.383283.
[26] Aditi Udupa, Xin Yu, Lonna Edwards, and Lynford L. Goddard, "Selective area formation of arsenic oxide-rich octahedral microcrystals during photochemical etching of n-type GaAs," *Optical Materials Express*, vol. 8, no. 2, pp. 289-294, 2018, doi; 10.1364/OME.8.000289.